Chemical Engineering Journal 162 (2010) 702–709

Contents lists available at ScienceDirect

Chemical Engineering Journal

journal homepage: www.elsevier.com/locate/cej

Photodegradation of Reactive Blue 4 solutions under ferrioxalate-assisted UV/solar photo-Fenton system with continuous addition of H_2O_2 and air injection

J.M. Monteagudo*, A. Durán, M. Aguirre, I. San Martín

University of Castilla-La Mancha, Grupo IMAES, Department of Chemical Engineering Escuela Técnica Superior de Ingenieros Industriales, Avda. Camilo José Cela, 1, 13071 Ciudad Real, Spain

ARTICLE INFO

Article history:
Received 17 February 2010
Received in revised form 19 May 2010
Accepted 22 June 2010

Keywords:
Blue 4
Ferrioxalate
Photo-Fenton
Neural networks
CPC

ABSTRACT

An experimental study based on the homogeneous ferrioxalate-assisted solar photo-Fenton process shows the effect of the continuous addition of hydrogen peroxide and air injection on the degradation of non-biodegradable dye Reactive Blue 4 (RB4) solutions. The reaction was carried out in a CPC (compound parabolic collector) solar pilot plant reactor. It was shown that the degree of dye solution mineralization was enhanced because the scavenger effect of H_2O_2 was minimized. Air bubbling had a negative effect because oxygen reacted with oxalyl radical anions, diminishing the amount of generated Fe(II), and consequently the concentration of hydroxyl radicals produced under irradiation of oxalate in the presence of peroxide was lower. In addition, this system permits the use of lower concentrations of ferrous ion, reducing the costs of the later iron removal process. Under the optimal conditions selected in this system, TOC removal was increased from 61% to 82% with a shorter reaction time as compared with a peroxide dose at the beginning of the reaction. The efficiency of the mineralization of RB4 solutions was enhanced when the solar CPC reactor worked together with an artificial UV-A/C pilot plant, increasing TOC removal up to 95%. Artificial UV lamps can be used either to improve the process or as an alternative to solar CPC on cloudy days.

1. Introduction

The textile industry produces large quantities of wastewaters containing high levels of organic and color contaminants. The color and toxicity of dyes influence the quality of life by causing health problems, in addition to influencing the efficiency of some water treatment techniques. To avoid the environmental impact produced by the discharge of these types of non-biodegradable toxic pollutants, an efficient treatment of these effluents needs to be developed.

Among the different advanced oxidation processes, the homogeneous solar photo-Fenton reaction is one of the most environmentally benign and cost-effective systems to generate hydroxyl radicals, •OH, and to degrade dye solutions, as previously reported [1,2]. Although H_2O_2 only uses photons below 350 nm (≈3% of solar irradiation), ferrioxalate, a photosensitive complex, can be used in addition in order to expand the usage of the solar spectrum range up to 450 nm (≈18% of solar irradiation), improving the oxidation efficiency of the solar photo-Fenton process [3–6]. Besides, the photolysis of ferrioxalate generates extra H_2O_2 for the Fenton reaction to yield more •OH radicals through a well-known mechanism [7,8], improving the degradation rate, as is indicated below.

In recent years, ferrioxalate has been used in the photo-Fenton reaction involving ferric compounds, but there is very little information on the ferrioxalate-assisted photo-Fenton system using ferrous-initiated processes. The use of ferrous sulphate is advantageous since it is less corrosive than ferric salts, very cheap and more soluble than ferric compounds.

RB4 was selected as model pollutant since their high consumption in textile industry has attracted the attention of the public and the authorities with respect to the toxicological and environmental aspects. As previously reported [1], the authors studied the ferrioxalate-assisted, solar photo-Fenton degradation of Reactive Blue 4 (RB4) solutions appearing in the manufacturing wastewaters of textile dyeing using a compound parabolic collector (CPC). Under the optimal conditions selected in that work ($[H_2O_2]$ = 120 ppm (with two additions during the reaction), [Fe(II)] = 7 ppm, $[(COOH)_2]$ = 10 ppm, pH 2.5), color was completely removed, whereas only 66% removal of total organic carbon (TOC) was reached. On the other hand, several problems arose:

(a) Two additions of H_2O_2 during the reaction were needed to guarantee that there was enough peroxide present in the water solution to achieve that degree of mineralization, although the radical scavenger effect of excess peroxide was detrimental to

* Corresponding author.
E-mail address: josemaria.monteagudo@uclm.es (J.M. Monteagudo).

1385-8947/$ – see front matter © 2010 Elsevier B.V. All rights reserved.
doi:10.1016/j.cej.2010.06.029

the photocatalytic process. Besides, this system is quite complex for industrial scale operations.

(b) The degradation efficiency of the solar installation on cloudy days was low.

To overcome these drawbacks, in this work, a series of experiments was carried out with continuous addition of H_2O_2 at a constant flow rate throughout the reaction (easier to operate on the industrial scale) to test if the radical scavenger effect could be minimized. In addition, we studied air bubbling in the reservoir tank during the reaction to find out if the degradation rate could be increased. The viability of using low iron concentrations to minimize the need for a later Fe removal process and thus reducing operation costs was also evaluated. Finally, the combination (in series) of an artificial UV-A/C pilot plant and the solar CPC pilot plant to increase the efficiency of the system was studied, particularly for cloudy days.

A multivariate experimental design was performed to study the effect of all the variables simultaneously (pH, air flow rate, H_2O_2 flow rate and initial concentrations of Fe(II) and oxalic acid). The results of the experimental tests were fitted using neural networks (NNs), which allows the values of the mineralization rate constant (response function) to be estimated within the studied range as a function of the process factors. Additionally, the saliency analysis of each variable in the NNs helps to discern the real relevance of all of them. The decrease of color, TOC, remaining H_2O_2 concentration and dissolved oxygen was monitored.

2. Experimental

2.1. Materials

RB4 ($C_{23}H_{14}Cl_2N_6O_8S_2$) (Fig. 1) solutions were prepared from pure compound purchased from Aldrich. $FeSO_4{\cdot}7H_2O$ (Panreac, analytical grade) and $(COOH)_2{\cdot}2H_2O$ (Panreac, 99.5%) were added to the wastewater to form ferrioxalate complexes that needed to be used in situ immediately because of their light sensitivity. Commercial hydrogen peroxide (30%, w/v, Merck) was added to the reactor after addition of Fe(II) and oxalic acid and pH adjustment. The pH was previously adjusted (between 2 and 6) by using 0.1 M H_2SO_4 and 6 M NaOH solutions. The initial concentration of dye was always 20 ppm.

When the irradiation started at time $t = 0$, an air stream was bubbled in the reservoir tank using a compressor (RIETSCHLE) coupled with a COMAQUINSA model R-005 rotameter.

The initial concentration of hydrogen peroxide in the water was always 50 ppm prior to continuous addition of H_2O_2 in each experiment. During the reaction, H_2O_2 was added through a needle (inner diameter, 3 mm) at a selected constant flow rate (between 0 and 1 mL min^{-1}) by means of a precision syringe pump (Terumo, model STC-521) coupled with a 60-mL syringe. The needle extended 70 cm into the reactor with the tip immersed in the liquid. At the end of the experiment, between 18 and 60 mL of peroxide solution has been added to the reactor. The small addition of H_2O_2 solution and the periodic removal of solution samples do not significantly change the volume of the reaction mixture (35 L). The effluent flow rate of the recirculation tank was 30 L min^{-1}. Before analysis, all of the samples were withdrawn from the reactor and immediately treated with excess Na_2SO_3 solution to prevent further oxidation.

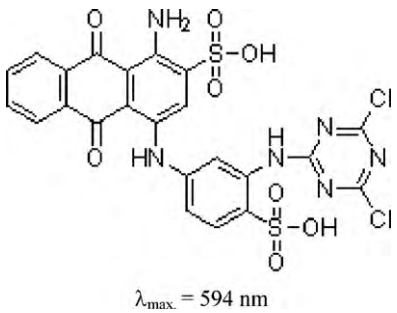

Fig. 1. RB4 chemical structure.

2.2. Photochemical reactions

2.2.1. Solar CPC pilot plant

The CPC plant (manufactured by ECOSYSTEM, S.A.) is composed of a solar reactor that consists of a continuously stirred tank (50 L), a centrifugal recirculation pump and a solar collector unit with an area of 2 m^2 (concentration factor = 1). This unit is housed in an aluminum frame mounted on a fixed south-facing platform tilted 39° (latitude of Ciudad Real, Spain) with respect to the horizontal plane and connecting the tubing and valves (Fig. 2). The total illuminated volume inside the 16 borosilicate-glass absorber tubes is 16 L. UV irradiation was measured by a radiometer (Ecosystem, model ACADUS-85), which facilitated the measurement of the received irradiation as UV-A (300–400 nm). The data – incident solar power (W m^{-2}) and accumulated solar energy (Wh) – are measured by means of a PLC (Programmable Logic Controller) coupled with the radiometer.

2.2.2. UV-A/C pilot plant

The UV pilot plant (FLUORACADUS-08/2.2) is also shown in Fig. 2, and it is composed of a 28-L reactor (2240 mm × 730 mm × 100 mm) with two UV-C lamps (200–280 nm, TUV_TL_D_55W_HO_SLV UV-C PHILIPS) and two UV-A lamps (320–400 nm, CLEO_Effect_70W_SLV PHILIPS). Both UV-C (for photolysis of H_2O_2) and UV-A (for ferrioxalate complexes photochemical reactions) were used at the same time.

2.3. Analysis

Changes in the RB4 concentration were determined from the absorbance at 594 nm using a UV–vis spectrophotometer (Zuzi 4418PC), because no intermediates that absorb in that wavelength range are formed, according to the absorption spectrum. The degree of mineralization analysis was followed by the TOC variation analysis. TOC was determined using a TOC-5050 Shimadzu analyzer (standard deviation < 0.2 mg L^{-1}).

The evolution of the concentration of H_2O_2 in the solution was obtained by titration through an aqueous solution of potassium permanganate (0.02 M) using an automatic Titrino SET/MET 702 (Metrohm). Dissolved O_2 concentration was measured using a luminescent dissolved oxygen (LDO) sensor.

2.4. Experimental design

A central composite experimental design was applied to investigate the effect of five variables (pH, air flow rate, H_2O_2 flow rate and initial concentrations of Fe(II) and oxalic acid) for the ferrioxalate-assisted solar photo-Fenton process with continuous addition of H_2O_2 and air injection (Table 1). "The initial concentration of RB4 was always 20 mg L^{-1}, and thus not considered as a factor. It is well known that an increase in the initial concentration of a contaminant compound decreases degradation efficiency because the path length of a photon entering the solution, and thus the amount of hydroxyl radicals generated, is decreased, so the probability of reaction is also decreased".

The design consists of three series of experiments [9]:

(i) a 2^k factorial design (all possible combinations of codified values +1 and −1), which in the case of $k = 5$ variables consists of 32 experiments (Experiments 1–32);

(ii) axial or star points (codified values $\alpha = 2^{k/4} = \pm 2.378$) consisting of $2^k = 10$ experiments (Experiments 33–42);

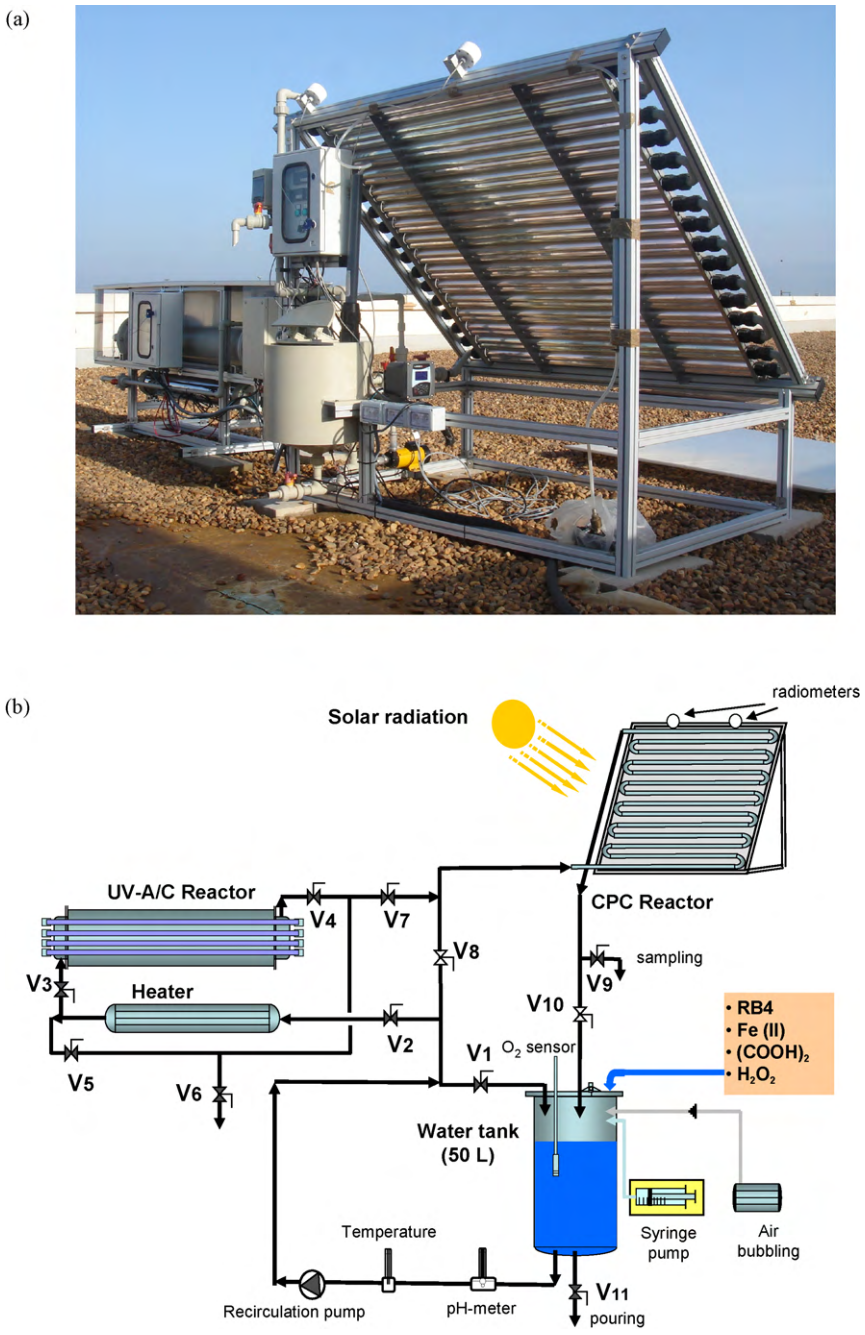

Fig. 2. Experimental set-up based on a CPC and an artificial UV-A/C pilot plant (a) photo, (b) scheme.

(iii) central points, i.e., replicates of the central point (four experiments, 43–46).

Temperature and incident solar power were not controlled during the experiment, but they were measured during the reaction so that their average values were included in the fitting.

In all of the experiments, the disappearance of TOC followed pseudo-first order kinetics with respect to the TOC concentration as follows:

$$r = -\frac{dC}{di} = k_m C \tag{1}$$

where r is the reaction rate, C is the concentration of total organic carbon (ppm) at an accumulated solar energy i (Wh) received by the water solution and k_m is the pseudo-first order mineralization kinetic rate constant ($W^{-1}\,h^{-1}$) for the photochemical reaction. This equation can be integrated between $i = 0$ and $i = i$, yielding:

$$\ln \frac{Co}{C} = k_m\ i \tag{2}$$

where Co is the initial concentration of TOC. According to this expression, a plot of the first term versus i must yield a straight line, validating Eq. (2) whose slope is k_m.

2.5. Neural network strategy

In this work, a linear basis function (linear combination between inputs, X_j, and weight factors, W_{ij}) was used. Each neural network is solved with two neurons and uses a simple exponential activation function [10]. The strategy is based on a back-propagation calculation. Parameters are found using the

Table 1
The 5-factor central composite design matrix. Ferrioxalate-assisted solar photo-Fenton system with continuous addition of H_2O_2 and air injection.

Experiment	H_2O_2 (mL min^{-1})	[Fe] (ppm)	Air flow rate O_2 (N m^3 h^{-1})	$[COOH]_2$ (ppm)	pH
1	0.71	10.65	1.31	42.61	4.84
2	0.29	10.65	1.31	42.61	4.84
3	0.71	4.35	1.31	42.61	4.84
4	0.29	4.35	1.31	42.61	4.84
5	0.71	10.65	0.89	42.61	4.84
6	0.29	10.65	0.89	42.61	4.84
7	0.71	4.35	0.89	42.61	4.84
8	0.29	4.35	0.89	42.61	4.84
9	0.71	10.65	1.31	17.39	4.84
10	0.29	10.65	1.31	17.39	4.84
11	0.71	4.35	1.31	17.39	4.84
12	0.29	4.35	1.31	17.39	4.84
13	0.71	10.65	0.89	17.39	4.84
14	0.29	10.65	0.89	17.39	4.84
15	0.71	4.35	0.89	17.39	4.84
16	0.29	4.35	0.89	17.39	4.84
17	0.71	10.65	1.31	42.61	3.16
18	0.29	10.65	1.31	42.61	3.16
19	0.71	4.35	1.31	42.61	3.16
20	0.29	4.35	1.31	42.61	3.16
21	0.71	10.65	0.89	42.61	3.16
22	0.29	10.65	0.89	42.61	3.16
23	0.71	4.35	0.89	42.61	3.16
24	0.29	4.35	0.89	42.61	3.16
25	0.71	10.65	1.31	17.39	3.16
26	0.29	10.65	1.31	17.39	3.16
27	0.71	4.35	1.31	17.39	3.16
28	0.29	4.35	1.31	17.39	3.16
29	0.71	10.65	0.89	17.39	3.16
30	0.29	10.65	0.89	17.39	3.16
31	0.71	4.35	0.89	17.39	3.16
32	0.29	4.35	0.89	17.39	3.16
33	1.00	7.50	1.10	30.00	4.00
34	0.00	7.50	1.10	30.00	4.00
35	0.50	15.00	1.10	30.00	4.00
36	0.50	0.00	1.10	30.00	4.00
37	0.50	7.50	1.60	30.00	4.00
38	0.50	7.50	0.60	30.00	4.00
39	0.50	7.50	1.10	60.00	4.00
40	0.50	7.50	1.10	0.00	4.00
41	0.50	7.50	1.10	30.00	6.00
42	0.50	7.50	1.10	30.00	2.00
43	0.50	7.50	1.10	30.00	4.00
44	0.50	7.50	1.10	30.00	4.00
45	0.50	7.50	1.10	30.00	4.00
46	0.50	7.50	1.10	30.00	4.00
(+α)	1.00	15.00	1.60	60.00	6.00
(−α)	0.00	0.00	0.60	0.00	2.00
(+1)	0.71	10.65	1.31	42.61	4.84
(−1)	0.29	4.35	0.89	17.39	3.16
(0)	0.50	7.50	1.10	30.00	4.00

solver tool in an in-house Excel spreadsheet and using the Marquardt non-linear fitting algorithm [11]. Further details can be found in literature [12]. Finally, a measure of the saliency of the input variables was made based upon the connection weights of the NNs [13]. This study allows the analysis of the relevance of each variable with respect to the others (expressed as a percentage).

3. Results and discussion

3.1. Solar photo-Fenton/ferrioxalate tests with continuous addition of H_2O_2 and air injection

To study the effect of the variables (peroxide flow rate, air flow rate, pH, and initial concentrations of Fe(II) and oxalic acid) on the response function (mineralization kinetic rate constant), experiments from a central composite design were performed. The complete experimental design matrix and variable ranges for the ferrioxalate-assisted solar photo-Fenton process with continuous addition of H_2O_2 and air injection are shown in Table 1. Since decoloration is a fast process and is completely achieved (95–99% color removal in 20 min, ≈40 Wh measured by radiometer) under the operation conditions tested herein, this experimental design was focused on the study of RB4 mineralization.

Experimental results and NNs predictions for the mineralization rate pseudoconstant (k_m) are in good agreement, with an average error lower than 11% (data not shown). The equation and parameters for the fitting of k_m are shown in Table 2. N_1 and N_2 are general factors related to the first and the second neuron, respectively. W_{11}–W_{17} are the contribution parameters to the first neuron and represent the influence of each of the seven variables in the process (H_2O_2 flow rate, $[Fe(II)]_o$, air flow rate, $[(COOH)_2]_o$, pH, average temperature and average incident solar power); W_{21}–W_{27} are the contributions to the second neuron and they are related to the same variables.

Table 2
Neural network fittings for the mineralization of RB4 solutions under the ferrioxalate-assisted solar photo-Fenton process with continuous addition of H_2O_2 and air injection: equation, parameters values and saliency analysis (%).

Neural network fitting		
Equation (see footnote)	k_m $[W^{-1}\,h^{-1}] = N_1 \times (1/(1 + 1/EXP(P \times W_{11} + F \times W_{12} + A \times W_{13} + O \times W_{14} + H \times W_{15} + T \times W_{16} + L \times W_{17})) + N_2 \times (1/(1 + 1/EXP(P \times W_{21} + F \times W_{22} + A \times W_{23} + O \times W_{24} + H \times W_{25} + T \times W_{26} + L \times W_{27})))$	
Weight factors	Parameter	Values of neurons and parameters to obtain the mineralization kinetic rate constant of dye solution, k_m
N_1	Neuron	0.460
W_{11}	H_2O_2 flow rate	−0.171
W_{12}	[Fe(II)]	−1.525
W_{13}	Air flow rate	−1.136
W_{14}	$[(COOH)_2]$	0.596
W_{15}	pH	−2.654
W_{16}	Temperature	0.003
W_{17}	Solar power	2.586
N_2	Neuron	−0.374
W_{21}	H_2O_2 flow rate	−0.186
W_{22}	[Fe(II)]	−1.946
W_{23}	Air flow rate	−1.319
W_{24}	$[(COOH)_2]$	0.587
W_{25}	pH	−2.479
W_{26}	Temperature	0.055
W_{27}	Solar power	3.203

Saliency analysis (%)

H_2O_2 flow rate	[Fe(II)]	Air flow rate	$[(COOH)_2]$	pH	Temperature	Solar power
2.37	22.63	16.18	7.95	12.68	0.31	37.88

Parameters values (P, F, A, O, H, T and L) in equations must be previously normalized to the (0.1) interval.
P = flow rate of hydrogen peroxide, mL min^{-1}; F = initial concentration of Fe(II), ppm; A = air flow rate, N m^3 h^{-1}; O = concentration of oxalic acid, ppm; H = pH; T = temperature (°C); typical range: ≈23.5–31.5 °C; L = solar power, W m^{-2}; typical range: ≈34–41 W m^{-2}.

The results of a saliency analysis of the input variables for each neural network (%) are also shown in Table 2. From these results, it is possible to deduce the effect of each parameter on the variable studied. It was confirmed that, over the studied ranges, incident solar power and initial concentration of [Fe(II)] are the most significant factors affecting the mineralization kinetics.

3.1.1. Effect of pH and H_2O_2 flow rate

Fig. 3a shows a simulation analysis example from NNs (equation shown in Table 2). The effects of the hydrogen peroxide flow rate and the pH on the value of the mineralization kinetic rate constant k_m (operating conditions: average temperature = 27.5 °C, $[Fe(II)]_o$ = 7 ppm, $[(COOH)_2]_o$ = 30 ppm, average solar power = 37 W m^{-2}, air flow rate = 1.6 N m^3 h^{-1}) can be seen. pH is an important parameter for photo-Fenton processes. It affects the generation of hydroxyl radicals and the nature of the iron species in solution [1]. When the pH is lower than 3–4, the predominant Fe(III) species are $[Fe(C_2O_4)_2]^-$ and $[Fe(C_2O_4)_3]^{3-}$, which are highly photoactive; under solar UV light they can effectively convert an Fe(III) ion into an Fe(II) ion via Eq. (3), and more •OH radicals are produced by the reaction of the generated ferrous ions with hydrogen peroxide [14,15]. However, when the pH value is increased to about 4–5, the Fe(III)-oxalate species are mainly $Fe(C_2O_4)^+$ and $[\equiv Fe(C_2O_4)]^+$, which are less photoactive, resulting in a lower mineralization rate. In addition, above these pH values, the degradation efficiency decreases since the coagulation of the Fe(III) complexes reduces the catalytic effect of Fe(II) to decompose H_2O_2.

$$[Fe(C_2O_4)_3]^{3-} + h\nu \rightarrow Fe(II) + 2\,C_2O_4^{2-} + C_2O_4^{\bullet -} \quad (3)$$

As can be seen in Fig. 3a, the H_2O_2 flow rate has a negligible effect on the mineralization rate over the studied experimental range, as already reflected in Table 2 (2.37% saliency analysis). In our previous work [1], the results of an analysis of the remaining H_2O_2 revealed that when peroxide was added at the beginning of the reaction, the amount of H_2O_2 in solution decreased from high values at the initial time to nearly disappearing after 80 Wh. Thus, initially, there was an excess of H_2O_2, and the well-known scavenger effect occurred. However, a new dose of peroxide was needed later to improve the degree of mineralization. In the present work, with continuous addition of H_2O_2, the measurements of peroxide in solution are typically constant and low during the reaction, which indicates that all added peroxide is consumed immediately. This negligible influence of the H_2O_2 flow rate (over the studied range) on k_m can be due to two balanced, opposite effects. On the one hand, the concentration of H_2O_2 in solution is increased when the peroxide flow rate increases and by generation during the photo-oxidation process in the presence of ferrioxalate [1] according to Eqs. (3)–(7) as a function of Fe and oxalic. On the other hand, peroxide is consumed by a reaction with Fe(II) to form •OH radicals via Eq. (8) and by self-decomposition according to Eq. (9). The results obtained in this work reveal that the peroxide scavenger effect (Eq. (10)) in this system is minimized, and the mineralization degree is enhanced up to 82% with respect to the process with addition of peroxide in two dosages (66% TOC removal) [1]. The values of k_m were obtained from TOC data between 0 and 40 Wh (the interval where mineralization obeys pseudo-first order kinetics). k_m does not depend on the flow rate of H_2O_2, but the results of TOC removal (%) obtained at the end of the reaction revealed that 0.29 mL min^{-1} was enough to reach the maximum value of 82% TOC removal.

$$C_2O_4^{\bullet -} + [Fe(C_2O_4)_3]^{3-} \rightarrow Fe(II) + 3\,C_2O_4^{2-} + 2CO_2 \quad (4)$$

$$C_2O_4^{\bullet -} + O_2 \rightarrow O_2^{\bullet -} + 2CO_2 \quad (5)$$

$$O_2^{\bullet -} + H^+ \rightarrow HO_2^{\bullet} \quad (6)$$

$$HO_2^{\bullet} + HO_2^{\bullet} \rightarrow H_2O_2 + O_2 \quad (7)$$

$$H_2O_2 + Fe(II) \rightarrow Fe(III) + {}^{\bullet}OH + OH- \quad (8)$$

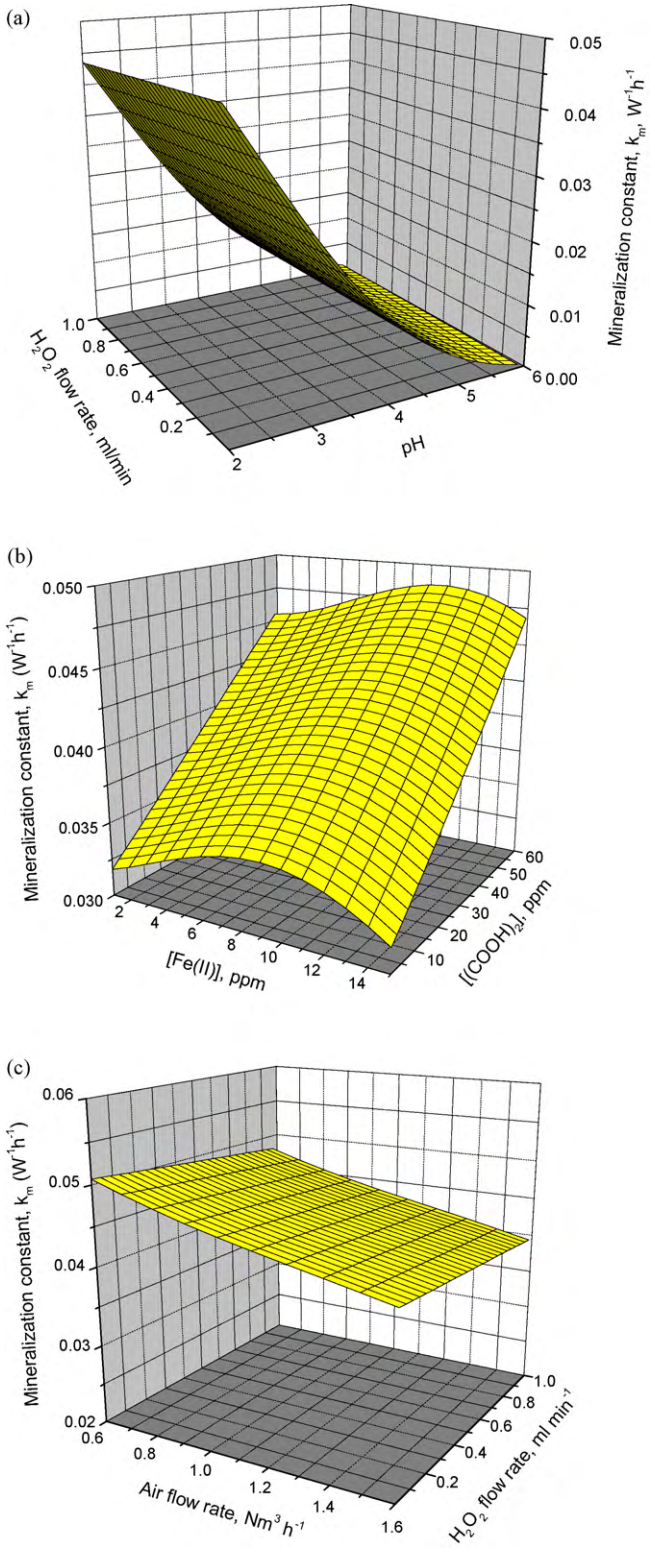

Fig. 3. NNs simulation of the influence of different variables on the mineralization kinetic rate constant, k_m. (a) Effect of the H_2O_2 flow rate and pH. Average temperature = 27.5 °C, $[Fe(II)]_o$ = 7 ppm, $[(COOH)_2]_o$ = 30 ppm, average solar power = 37 W m^{-2}, air flow rate = 1.6 N m^3 h^{-1}). (b) Effect of the initial concentration of Fe(II) and oxalic acid. (Average temperature = 27.5 °C, H_2O_2 flow rate = 0.5 mL min^{-1}, average solar power = 37 W m^{-2}, air flow rate = 1.6 N m^3 h^{-1}, pH 2). (c) Effect of H_2O_2 flow rate and air bubbling. (Average temperature = 27.5 °C, $[Fe(II)]_o$ = 7 ppm, $[(COOH)_2]_o$ = 30 ppm, average solar power = 37 W m^{-2}, pH 2).

$$2H_2O_2 \rightarrow O_2 + 2H_2O \quad (9)$$

$$H_2O_2 + {}^{\bullet}OH \rightarrow HO_2{}^{\bullet} + H_2O \quad (10)$$

3.1.2. Effect of initial concentrations of Fe(II) and oxalic acid

Fig. 3b shows (as an example) the effect of the initial concentrations of oxalic acid and Fe(II) on k_m, as simulated by NNs (operating conditions: average temperature = 27.5 °C, H_2O_2 flow rate = 0.5 mL min^{-1}, average solar power = 37 W m^{-2}, air flow rate = 1.6 N m^3 h^{-1}, pH 2). For each value of the initial oxalic acid concentration, there is an optimal value of ferrous ion. The maximum degradation rate is reached at $[(COOH)_2]$ = 60 ppm and [Fe(II)] = 12 ppm, which corresponds to a molar ratio of $(COOH)_2$:Fe close to 3, when the Fe(III) ions were complexed with the maximum amount of oxalate in the form of the saturated complex $Fe(C_2O_4)_3{}^{3-}$ (ferric iron complexed with three oxalate molecules as its limit load). However, when the molar ratio is below 3, insufficient oxalate is present, reducing the yield of Fe(II) ion regeneration. In addition, when an excess of Fe(II) is used, an inhibition effect is observed due to Fe(II) and Fe(III) competing for different radicals to form intermediates, as shown in Eqs. (11)–(13).

$$Fe(II) + {}^{\bullet}OH \rightarrow Fe(II) + OH^- \quad (11)$$

$$Fe(II) + HO_2{}^{\bullet} \rightarrow Fe(III)(HO_2)^{2+} \quad (12)$$

$$Fe(III) + O_2{}^{\bullet -} + H^+ \rightarrow Fe(III)(HO_2)^{2+} \quad (13)$$

Previous tests (data not shown) showed that an excess of oxalate (concentration of oxalic acid above 60 ppm) cannot complex with more ferric ions in solution, and the light penetration through irradiated wastewater decreases. In addition, the excess of oxalate acts as an additional organic compound, and so it competes with the hydroxyl radicals for the RB4 dye, reducing the degradation efficiency. On the other hand, similar results for TOC removal (%) (at the end of the reaction) were obtained using different amounts of oxalic acid and Fe(II) but maintaining the molar relation $[COOH)_2/[Fe(II)] \approx 3$. Thus, the lowest initial concentrations to obtain 82% TOC removal were 19 ppm oxalic acid and 4 ppm Fe(II). This system permits the use of lower concentrations of ferrous ion, which reduces the costs of the later iron removal process.

3.1.3. Effect of air bubbling

Fig. 3c shows the effect of the H_2O_2 flow rate and the air flow rate on k_m (operating conditions: average temperature = 27.5 °C, [Fe(II)] = 7 ppm, $[(COOH)_2]$ = 30 ppm, average solar power = 37 W m^{-2}, pH 2). As can be seen, air injection into the reactor had a negative effect on the mineralization rate in all of the ranges of peroxide flow rate studied.

To explain this behavior, Fig. 4 shows measurements of the oxygen concentration dissolved in water during the reaction, together with RB4 decoloration data for a typical test. It can be observed that a brief drop in the dissolved oxygen concentration takes place in the early stage of the reaction. As the reaction progresses, the dissolved oxygen increases until a maximum value is reached, and afterwards, it starts to decline. The decrease of dissolved O_2 could be due to the reaction of O_2 with the oxalyl radical anion, $C_2O_4{}^{\bullet -}$, according to Eq. (5) and with the intermediate organoradicals according to Eq. (14), in agreement with other researchers [16,17]. After 10 Wh of accumulated solar energy, the dissolved oxygen concentration increased via the ferrioxalate photochemistry (Eqs. (3)–(7)), by H_2O_2 decomposition (Eq. (9)) and by catalytic reactions of Fe(III) with either $HO_2{}^{\bullet}$ or H_2O_2 according to Eqs. (15) and (16). The further low-level depletion of O_2 at the end of the process could be due to the reaction of O_2 with the remaining organoradicals [16]. Both oxygen depletion and formation reactions occur throughout the process. Depending on the availability of the reagents and some

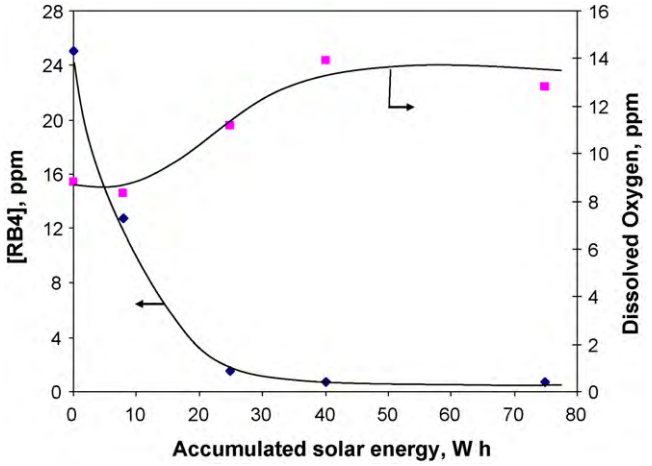

Fig. 4. Changes in the RB4 concentration and dissolved oxygen in a typical test (H_2O_2 flow rate = 0.71 mL min^{-1}, [Fe(II)]$_o$ = 4.35 ppm, air flow rate = 0.89 N m^3 h^{-1}, [(COOH)$_2$]$_o$ = 17.39 ppm, pH 2, average solar power = 56.3 W m^{-2}, average temperature = 27.3 °C).

other factors, one of the reactions becomes dominant at different stages of the reaction.

$$R^{\bullet} + O_2 \rightarrow RO_2^{\bullet} + H_2O \rightarrow ROH + HO_2^{\bullet} \quad (14)$$

$$Fe(III) + HO_2^{\bullet} \rightarrow Fe(II) + O_2 + H^+ \quad (15)$$

$$Fe(III) + 2H_2O_2 \rightarrow Fe(II) + O_2 + 2H_2O \quad (16)$$

Thus, when oxygen is injected into the solution, reaction (5) diminishes the amount of oxalyl radical anion that could decompose to the carbon dioxide radical anion, $CO_2^{\bullet -}$, according to Eq. (17). This reducing agent could produce Fe(II) via Eq. (18) [18,19], and extra $^{\bullet}$OH radicals could be generated when ferrioxalate is irradiated in the presence of H_2O_2 and Fe(II) via Eq. (19) [20]. Thus, the degradation efficiency is higher without air bubbling in the studied range and so the costs of energy could be reduced.

$$C_2O_4^{\bullet -} \rightarrow CO_2^{\bullet -} + CO_2 \quad (17)$$

$$CO_2^{\bullet -} + Fe(III)(C_2O_4)_3^{3-} \rightarrow Fe(II) + CO_2 + 3\,C_2O_4^{2-} \quad (18)$$

$$Fe(II) + H_2O_2 + 3\,C_2O_4^{2-} \rightarrow Fe(III)(C_2O_4)_3^{3-} + OH^- + {}^{\bullet}OH \quad (19)$$

On the other hand, as can be seen in Fig. 3c, an increase in the flow rate of H_2O_2 slightly decreased the value of k_m, possibly due to the scavenger effect of a small amount of excess peroxide according to Eq. (10) in these operation conditions.

3.1.4. Selected conditions

According to the results discussed above, and taking into account that the aim is to obtain good mineralization efficiency at the end of the experiments, the following conditions were selected: H_2O_2 flow rate = 0.29 mL min^{-1}, [Fe(II)] = 4 ppm, [(COOH)$_2$] = 19 ppm, pH 2 and no air injection.

3.2. Comparative study

Fig. 5 compares the degree of mineralization in RB4 solutions under the optimal conditions selected in this research with the same conditions modified with the addition of hydrogen peroxide at the beginning of the reaction.

TOC removal increased from 61% to 82% (160 Wh accumulated solar energy), which indicates an increase of the photodegradation efficiency. Moreover, it is also remarkable that under the conditions selected in this work, the amounts of peroxide and Fe(II) used were smaller, and air injection was not necessary. In addition, oxalic acid

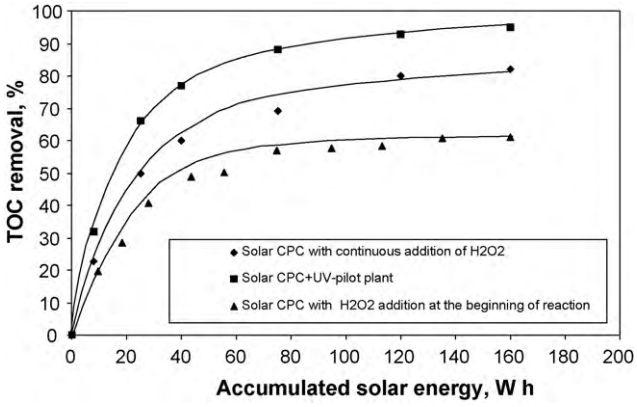

Fig. 5. Comparison of mineralization under different conditions: (♦) best conditions selected in this research (H_2O_2 flow rate = 0.29 mL min^{-1}, [Fe(II)]$_o$ = 4 ppm, [(COOH)$_2$]$_o$ = 19 ppm, pH 2, no air bubbling). (▲) Addition of H_2O_2 at the beginning, ([H_2O_2]$_o$ = 250 ppm, [Fe(II)]$_o$ = 4 ppm, [(COOH)$_2$]$_o$ = 19 ppm, pH 2, no air bubbling). (■) Use of a solar CPC reactor working together with the UV-A/C reactor.

could also be used for pH adjustments. Thus, it is important to point out that this system reduces the costs of electric power, chemicals and removal of Fe ions at the end of the treatment.

3.3. Effect of using a UV-A/C reactor in series with the solar CPC reactor

Fig. 5 also shows the results obtained for the mineralization of RB4 solutions when the solar CPC reactor is working together with the UV-A/C reactor as described in Section 2.2.2. The results show that the degradation efficiency was considerably increased, since TOC removal was increased up to 95%, and the process was faster as compared with single solar system. This result is due to the continuous regeneration of Fe(II) via the photoreduction of Fe(III) with 200–400 nm UV-C light and the extra generation of new $^{\bullet}$OH radicals with H_2O_2 as well as by the photochemical reactions of ferrioxalate complexes using UV-A radiation as indicated above. The degradation of Blue 4 solutions was again carried out under the same selected conditions shown in Section 3.1.4, but this time with only artificial UV-A/C light irradiation, as the solar power was below 10 W m^{-2} (a typical cloudy day). 90% TOC removal (data not shown) was achieved which indicates that UV lamps can be used either to improve the process (reducing more TOC or operating faster) or as an alternative to the solar CPC on cloudy days.

4. Conclusions

The degree of mineralization of dye solutions was enhanced when hydrogen peroxide was continuously dosed because the scavenger effect of H_2O_2 was minimized. Air bubbling had a negative effect because less Fe(II) and $^{\bullet}$OH radicals were generated. Oxalic acid improved RB4 solution mineralization significantly, because ferrioxalate complexes absorb strongly and a higher portion of the solar spectrum was used.

Under the conditions selected in this work (H_2O_2 flow rate = 0.29 mL min^{-1}, [Fe(II)] = 4 ppm, [(COOH)$_2$] = 19 ppm, pH 2, and no air bubbling), the efficiency of the mineralization process was increased from 61% (with addition of H_2O_2 at the beginning of the reaction) up to 82% (with a shorter reaction time). In contrast, the efficiency of decoloration and the mineralization of RB4 solutions were enhanced when the solar CPC reactor worked together with an artificial UV-A/C pilot plant. Under the optimal conditions, TOC removal was increased up to 95%.

This system permits the use of a low concentration of Fe(II), and oxalic acid can also be used for pH adjustment, reduc-

ing the operating costs of later iron removal, chemicals and manpower.

Acknowledgement

Financial support from the Consejería de Educación y Ciencia of the Junta de Comunidades de Castilla-La Mancha (PCI08-0047-4810) is gratefully acknowledged.

References

[1] A. Durán, J.M. Monteagudo, E. Amores, Solar photo-Fenton degradation of Reactive Blue 4 in a CPC reactor, Appl. Catal. B: Environ. 80 (2008) 42–50.
[2] S. Malato, J. Blanco, J. Cáceres, A.R. Fernández-Alba, A. Agüera, A. Rodríguez, Photocatalytic treatment of water-soluble pesticides by photo-Fenton and TiO_2 using solar energy, Catal. Today 76 (2002) 209–220.
[3] S. Malato, J. Blanco, M.I. Maldonado, P. Fernández, D. Alarcón, M. Collares, J. Farinha, J. Correia de Oliveira, Engineering of solar photocatalytic collectors, Sol. Energy 77 (2004) 513–524.
[4] R. Bauer, G. Waldner, H. Fallmann, S. Hager, H. Karé, T. Krutzler, S. Malato, P. Maletzky, The photo-Fenton reaction and the TiO_2/UV process for waste water treatments – novel developments, Catal. Today 53 (1999) 131–144.
[5] R.F.P. Nogueira, A.G. Trovó, D.F. Mode, Solar photodegradation of dichloroacetic acid and 2,4-dichlorophenol using an enhanced photo-Fenton process, Chemosphere 48 (2002) 385–391.
[6] M.S. Lucas, J.A. Peres, Degradation of Reactive Black 5 by Fenton/UV-C and ferrioxalate/H_2O_2/solar light processes, Dyes Pigm. 74 (2007) 622–629.
[7] A. Safarzadeh-Amiri, J.R. Bolton, S.R. Cater, Ferrioxalate-mediated photodegradation of organic pollutants in contaminated water, Water Res. 31 (1997) 787–798.
[8] K. Selvam, M. Muruganandham, M. Swaminathan, Enhanced heterogeneous ferrioxalate photo-Fenton degradation of reactive orange 4 by solar light, Sol. Energy Mater. Sol. Cells 89 (2005) 61–74.
[9] G.E.P. Box, W.G. Hunter, J.S. Hunter, Statistics for Experimenters: An Introduction to Design, Data Analysis and Model Building, Wiley, New York, 1978.
[10] D.P. Morgan, C.L. Scofield, Neural Networks and Speech Processing, Kluwer Academic Publishers, London, 1991.
[11] D.W. Marquardt, An algorithm for least squares estimation of nonlinear parameters, J. Soc. Ind. Appl. Math. 11 (1963) 431–441.
[12] A. Durán, J.M. Monteagudo, M. Mohedano, Neural networks simulation of photo-Fenton degradation of Reactive Blue 4, Appl. Catal. B: Environ. 65 (2006) 127–134.
[13] R. Nath, B. Rajagopalan, R. Ryker, Determining the saliency of input variables in neural network classifiers, Comput. Oper. Res. 24 (1997) 767–773.
[14] M.E. Balmer, B. Sulzberger, Atrazine degradation in irradiated iron/oxalate systems: effects of pH and oxalate, Environ. Sci. Technol. 33 (1999) 2418–2424.
[15] F.B. Li, X.Z. Li, X.M. Li, T.X. Liu, J. Dong, Heterogeneous photodegradation of bisphenol A with iron oxides and oxalate in aqueous solution, J. Colloid Interface Sci. 311 (2007) 481–490.
[16] K.A. Hislop, J.R. Bolton, The photochemical generation of hydroxyl radicals in the UV–vis/ferrioxalate/H_2O_2 system, Environ. Sci. Technol. 33 (1999) 3119–3126.
[17] A. Aris, P.N. Sharrat, Influence of initial dissolved oxygen concentration on Fentonïs reagent degradation, Environ. Technol. 27 (2006) 1153–1161.
[18] G.D. Cooper, B.A. Degraff, On the photochemistry of ferrioxalate system, J. Phys. Chem. 75 (1971) 2897–2902.
[19] G.D. Cooper, B.A. Degraff, Photochemistry of the monoxalatoiron(III) ion, J. Phys. Chem. 76 (1972) 2618–2625.
[20] R.G. Zepp, B.C. Faust, J. Hoigné, Hydroxyl radical formation in aqueous reactions (pH 3–8) of iron(II) with hydrogen peroxide: the photo-Fenton reaction, J. Environ. Sci. Technol. 26 (1992) 313–319.